ASMS

FOCUS: APPLICATION OF PHOTONS AND RADICALS FOR MS:
RESEARCH ARTICLE

Structural Investigation of the Hormone Melatonin and Its Alkali and Alkaline Earth Metal Complexes in the Gas Phase

Satrajit Chakrabarty,[1,2] Matthew J. DiTucci,[1] Giel Berden,[3] Jos Oomens,[3,4] Evan R. Williams[1]

[1]Department of Chemistry, University of California, B-42 Hildebrand Hall, Berkeley, CA 94720, USA
[2]Laboratory of Physical Chemistry, Vladimir Prelog Weg 2, 8093, Zurich, Switzerland
[3]Institute for Molecules and Materials, FELIX Laboratory, Radboud University Nijmegen, Toernooiveld 7c, 6525 ED, Nijmegen, The Netherlands
[4]Van't Hoff Institute for Molecular Sciences, University of Amsterdam, Science Park 904, 1098 XH, Amsterdam, The Netherlands
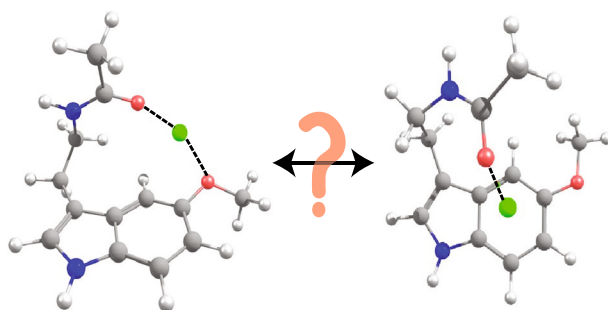
Abstract. Gas phase infrared dissociation spectra of the radical cation, deprotonated and protonated forms of the hormone melatonin, and its complexes with alkali (Li^+, Na^+, and K^+) and alkaline earth metal ions (Mg^{2+}, Ca^{2+}, and Sr^{2+}) are measured in the spectral range 800–1800 cm^{-1}. Minimum energy geometries calculated at the B3LYP/LACVP++** level are used to assign structural motifs to absorption bands in the experimental spectra. The melatonin anion is deprotonated at the indole-N. The indole-C linking the amide chain is the most favored protonation site. Comparisons between the experimental and calculated spectra for alkali and alkaline earth metal ion complexes reveal that the metal ions interact similarly with the amide and methoxy oxygen atoms. The amide I band undergoes a red shift with increasing charge density of the metal ion and the amide II band shows a concomitant blue shift. Another binding motif in which the metal ions interact with the amide-O and the π-electron cloud of the aromatic group is identified but is higher in energy by at least 18 kJ/mol. Melatonin is deprotonated at the amide-N with Mg^{2+} and the metal ion coordinates to the amide-N and an indole-C or the methoxy-O. These results provide information about the intrinsic binding of metal ions to melatonin and combined with future studies on solvated melatonin-metal ion complexes may help elucidate the solvent effects on metal ion binding in solution and the biochemistry of melatonin. These results also serve as benchmarks for future theoretical studies on melatonin-metal ion interactions.

Keywords: Melatonin-metal ion interaction, Ion spectroscopy, Free electron laser, Infrared spectroscopy, Infrared multiphoton dissociation

Correspondence to: Satrajit Chakrabarty;
e-mail: satrajit.chakrabarty@phys.chem.ethz.ch, Evan Williams;
e-mail: erw@berkeley.edu

Introduction

Melatonin, or *N*-acetyl-5-methoxytryptamine (Figure 1), is a hormone secreted by the pineal gland that carries out several essential functions in the human body. Its biosynthesis occurs through the uptake of tryptophan in pineal cells [1]. Melatonin plays a role in regulating sleep cycles [2], circadian rhythm [3], and blood pressure [4] and can also act as an antidepressant [5]. The amount of melatonin secreted decreases
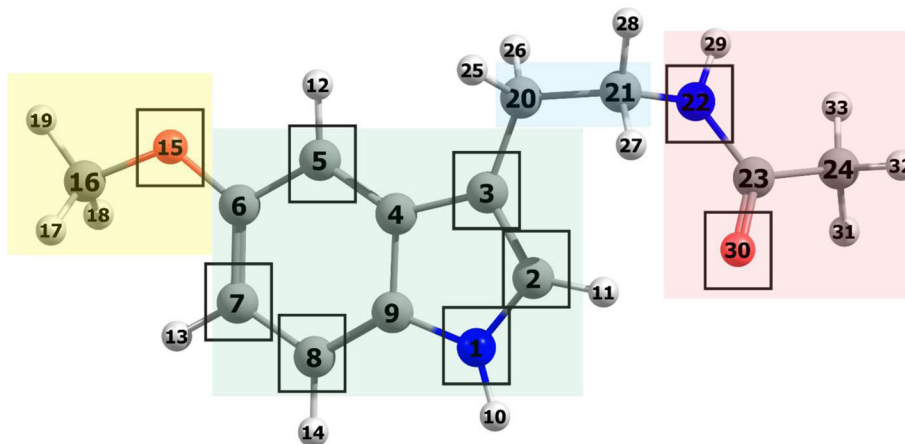
Figure 1. The melatonin molecule showing the numerical labeling of atoms used throughout the discussion. The four subunits of the molecule highlighted are methoxy group (yellow), indole unit (green), methylene unit (blue), and amide group (red). The atoms enclosed in the black boxes are the potential sites of protonation for which vibrational spectra were computed to compare to the measured spectrum of $[Mel + H]^+$

with age and often leads to sleep disorders in the elderly. Supplemental melatonin is often used to aid sleep and adaptation to altered day and night patterns. Endogenous melatonin is also an antioxidant [6], and it assists in protecting nuclear DNA, proteins, and membrane lipids by sequestration of superoxide anions, hydroxide radicals, and metal ions that generate reactive oxygen and nitrogen species [7]. The detrimental effects of several metal ions on the human body and how melatonin administration can achieve reduced levels of these ions and free radicals that the metal ions can generate has been recently reviewed [8].

The extent to which melatonin interacts with metal ions in aqueous solution has been investigated by adsorptive cathodic stripping voltammetry. Metal ions that bind to melatonin to varying extents include Fe^{3+}, Co^{2+}, Zn^{2+}, Cd^{2+}, Cu^{2+}, Li^+, K^+, and Na^+ [9–14]. Conversely, the interaction between Ca^{2+} and melatonin was reported to be unfavorable [13], although a reason for this was not discussed. Ion-ligand binding rules for organometallics, such as the 18-electron rule, have been proposed as a source for metal-dependent binding motifs. It is possible that metal ions adopt an η^6-hapticity chelation with the π-electron cloud of the benzene ring [13], but the exact binding motifs of metal ions with melatonin remain unknown. Metal ions can interact with melatonin through a number of coordination sites. The amide-O [15–19], the π-electron cloud of the benzene ring in the indole group [20], and the methoxy-O are most likely to coordinate with metal ions. Depending on the size and charge of the ion, characteristic infrared absorption bands of the different functional groups of melatonin are expected to undergo shifts in frequencies depending on the nature of interaction with a metal ion and exhibit different intensities compared to the bare molecule.

The neutral melatonin molecule has been characterized by various spectroscopic approaches. The conformers of neutral melatonin in a supersonic jet have been characterized using various two photon methods via electronic and vibrational spectroscopy in the C–H stretch region [21]. More recently,

the rotationally resolved electronic spectra of two conformers of neutral melatonin were reported [22]. Although a gas phase IR spectrum of melatonin or its associated complexes have not been measured in the amide I and amide II regions, previous IR spectra measured in the condensed phase have been reported for neutral melatonin between 100 and 3600 cm^{-1} [23, 24]. The earliest reported IR spectrum of melatonin is available on the NIST website [25]. Furthermore, the IR spectrum of melatonin in KBr pellets was measured by Bayari et al. [23] and Singh et al. [24] in the range between 100 and 4000 cm^{-1}. The region between 900 and 1700 cm^{-1} is characterized by C–C, C–N, and C=O stretches and C–H and N–H bends. The spectrum is rather complex due to several vibrational modes contributing to the measured bands. Amide I and II bands are observed at 1624 and 1488 cm^{-1}, respectively. (Note that Bayari et al. incorrectly assigned the band at 1555 cm^{-1} as the amide II band, possibly due to the low level of theory used). The C–O stretching band of the methoxy unit coupled to the CH$_3$ rocking motion occurs at 1175 cm^{-1}. Dunbar et al. have reported on the infrared multiple photon dissociation (IRMPD) spectra of metal ion complexes with dialanine and trialanine [26]. They observed a red shift of the amide I band and a blue shift of the amide II band for the polyalanine-metal complexes compared to bare polyalanine, with larger shifts associated with stronger ion-metal interactions. Similar trends are to be expected in the spectra of melatonin metal ion complexes, provided the amide group participates in binding the metal ions. Similar to the observed shifting for polyalanine complexes, shifts in the melatonin C–O stretching band can be used to identify metal ion-melatonin interactions. The band associated with the indole N–H in-plane bending has been observed at 1225 cm^{-1} with weak intensity in the spectrum of neutral melatonin [24] and is another characteristic vibration for identifying structural changes. Other bands observed in the spectrum arise from excitation of the indole ring C–C and C–N stretches as well as C–H bends of the indole ring, methylene, amide, and methoxy groups.

The site of protonation in protonated melatonin has been investigated earlier using different ionization methods and collision-induced dissociation coupled with quantum chemical calculations [27]. The different fragmentation pathways observed were rationalized in terms of protonation occurring at multiple energetically competitive sites including the C2, C5, C7, and O30 atoms. Other protonation sites considered by Bongiorno et al. were the N1 and O15 atoms, but quantum chemical calculations indicated these sites are energetically unfavorable. The most probable site identified is the C5 carbon atom.

In the present study, we use IRMPD to spectroscopically characterize both the protonation and metal binding sites for melatonin. We have also measured spectra of cationic and anionic melatonin, which are possible reaction intermediates in the metal scavenging reactions of melatonin. Comparisons of the experimental spectra to results from computations are used to elucidate details about metal ion binding of melatonin. The structural analysis presented in this work shows the functional groups of melatonin that interact with metal ions, and these results will serve as a reliable model to understand the biochemistry of melatonin-metal systems in biological systems.

Experimental

The spectroscopic measurements were performed at the FELIX Laboratory in Nijmegen, Netherlands [28]. The apparatus consists of an electrospray ion source coupled to a 4.7-T Fourier transform ion cyclotron resonance (FTICR) mass spectrometer. A 2 mM melatonin, Mel, stock solution and 5 mM metal salt solutions were prepared in 1:1 methanol/water mixtures. Electrospray ionization of 1:1 mixtures of the melatonin and the metal salt solutions were used to generate melatonin-metal ion complexes in the gas phase. The melatonin radical cation, $Mel^{+\bullet}$, was generated via electrospray ionization of a solution containing melatonin and copper sulfate. The copper ion undergoes efficient reduction to generate the melatonin radical cation. Deprotonated melatonin, $[Mel - H]^-$, was obtained by spraying 2 mM melatonin solution with 2% v/v 1 M KOH. The protonated melatonin ion, $[Mel + H]^+$, was generated by adding 2% v/v 1 M HCl to the 2 mM solution of melatonin. For the $[Mel + Ca]^{2+}$ complex, the initial melatonin-calcium salt solution was further diluted twofold with acetonitrile to suppress formation of the $[Mel_2 + Ca]^{2+}$ complex upon ionization. Upon electrospray ionization of this solution, the complex $[Mel + Ca]^{2+}(CH_3CN)$ was generated. The complex fragmented by loss of the CH_3CN molecule when irradiated with 10.6 μm light from a CO_2 laser for 0.25 s to form $[Mel + Ca]^{2+}$ in the FTICR trap. This approach proved to be effective in generating appreciable yields of the $[Mel + Ca]^{2+}$ complex.

The ions were accumulated in a hexapole ion trap for up to 5 s. The ions were then transferred through octopole ion guides to the FTICR cell, where ions of interest were mass selected by stored waveform inverse Fourier transform and then irradiated

with 10–45 laser pulses from the FELIX free electron laser (frequency, 600–1800 cm^{-1}; pulse energy, 10–60 mJ; bandwidth, 0.5% of center frequency). Upon resonant absorption, ions photodissociate and the photoproducts remain trapped along with the remaining precursor ions. Multiple dissociation channels related to loss of functional groups from melatonin were observed for all ions except complexes of melatonin with Na^+ and K^+, for which the only dissociation channel observed was the loss of the metal ions. The photodissociation rate constants (k_{IRMPD}) are calculated from the relation: $k_{IRMPD} = -(1 / t) \cdot [\ln(\sum \text{precursor ion abundance} / \sum(\text{precursor and product ion abundances}))]$, where t is the irradiation time. The IRMPD spectrum is obtained by plotting k_{IRMPD} as a function of the photon frequency, with each data point being an average of three to four measurements and being linearly corrected for laser power fluctuations. For the complexes of melatonin with Na^+ and K^+, the loss of the metal ions was the only fragmentation observed and the abundance of these metal ions varied significantly from scan to scan. Therefore, the IRMPD spectra of these two ions were obtained by monitoring frequency dependent depletion of the precursor ion.

Numbering for atoms in Mel that will be used throughout the discussion is provided in Figure 1. The molecule has been subdivided into four sections in order to facilitate discussion of characteristic vibrations pertaining to the methoxy group (yellow), indole unit (green), methylene carbon atoms (blue), and the amide group (red). The black squares around O15, C5, C7, C8, C3, C2, N1, N22, and O30 indicate the atoms that have been considered as potential sites of protonation.

Computational

Initial conformational searches were carried out using MacroModel 9.1 (Schrödinger Inc., Portland, OR, USA) with the OPLS2005 force field to generate up to 1000 structures. These initial geometries were grouped into families depending on similarities of the structures and a representative member of each family was chosen for further analysis using ab initio calculations. The chosen structures were geometry optimized at the B3LYP/LACVP++** level of theory using QChem v. 4.3.2 (Q-Chem, Inc., Pittsburgh, PA) [29]. Frequency calculations were done at the same level of theory using the optimized geometries. The zero-point energy, enthalpy, and entropy corrections at 298 K were calculated for these structures using unscaled B3LYP/LACVP++** harmonic oscillator frequencies. The calculated frequencies were scaled by 0.98 for comparison to the measured spectra of $Mel^{+\bullet}$, $[Mel - H]^-$, and $[Mel + H]^+$. The calculated frequencies of Mel complexes with the alkali metal and alkaline earth metal ions are scaled by 0.97 and 0.96, respectively. For Mel complexes with Mg^{2+}, frequency scaling factors of 0.96 and 0.93 were used for deprotonation at amide-N and indole-N, respectively. The scaling factors were chosen based on the frequency difference between the measured and calculated amide I bands. Although the correlations between measured and calculated spectra are satisfactory in most cases, computed band positions and intensities might

differ from experimentally measured values because of several factors. For example, anharmonic effects that are not taken into account by harmonic calculations often lead to differences in absorption frequencies and band intensities between experimental IRMPD and calculated spectra. Moreover, multiphoton dissociation is a nonlinear process that can lead to differences between the experimental and calculated linear absorption spectra. These differences have been discussed in details elsewhere [30]. All calculated spectra were convolved with a full width half maximum Gaussian profile of 25 cm^{-1}. A conformer for neutral melatonin was also geometry optimized at the same level of theory. The resultant bond lengths in the optimized structure compare well with experimentally determined values from crystal structures [31, 32]. This geometry does not represent the global minimum in conformational space and is used only to compare the bond lengths of this structure with optimized geometries of the Mel-metal ion complexes for which experimental IRMPD spectra were measured.

Results and Discussion

Spectra of Mel$^{+\bullet}$, [Mel − H]$^{−}$, and [Mel + H]$^{+}$

The spectra of Mel$^{+\bullet}$, [Mel − H]$^{−}$, and [Mel + H]$^{+}$ are shown in Figure 2(a)–(c), respectively. At the high frequency end of the spectra, an intense sharp band is observed in the spectra of Mel$^{+\bullet}$ and [Mel − H]$^{−}$ at 1678 cm^{-1}. Several overlapping bands are observed in the spectrum of [Mel + H]$^{+}$ between 1540 and 1725 cm^{-1}. Between 1000 and 1540 cm^{-1}, several intense bands occur in the spectra of Mel$^{+\bullet}$ and [Mel + H]$^{+}$, whereas the spectrum of [Mel − H]$^{−}$ has relatively weak although distinct absorptions in this region. Below 1000 cm^{-1}, only weak

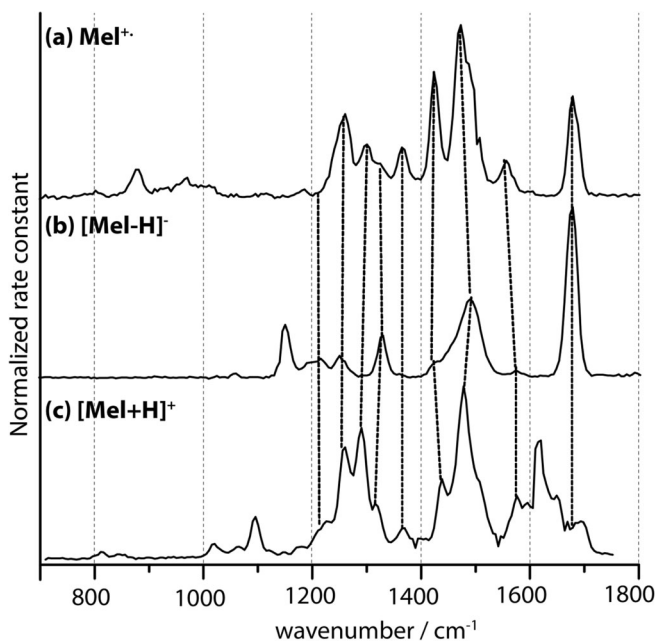**Figure 2.** IRMPD spectra of (**a**) Mel$^{+\bullet}$, (**b**) [Mel − H]$^{−}$, and (**c**) [Mel + H]$^{+}$. The dashed lines are added to facilitate comparison of absorption bands between the three ions

absorptions are observed in the spectra of Mel$^{+\bullet}$ and [Mel + H]$^{+}$ and none are observed in the spectrum of [Mel − H]$^{−}$.

There are at least three overlapping bands in the spectrum of [Mel + H]$^{+}$ between 1600 and 1800 cm^{-1} compared to the single intense peak at 1678 cm^{-1} in the spectra of Mel$^{+\bullet}$ and [Mel − H]$^{−}$. Based on earlier literature [26, 33, 34], the band at 1678 cm^{-1} is assigned to the amide CO stretch (amide I) absorption. The absence of an absorption band that can be clearly attributed to the amide I band in the spectrum of [Mel + H]$^{+}$ suggests that there is an interaction between the amide group and the proton. The band maxima are listed in Table 1 with the rows corresponding to the motifs. The low intensities or sometimes missing bands in the spectrum of [Mel − H]$^{−}$ could indicate the absence of structural motifs that are present in Mel$^{+\bullet}$ and [Mel + H]$^{+}$. Below 1500 cm^{-1}, the spectra of Mel$^{+\bullet}$ and [Mel + H]$^{+}$ have bands whose absorption frequencies differ by no more than 15 cm^{-1}. Peak positions differ by more than 50 cm^{-1} below 1200 cm^{-1} in the spectra of Mel$^{+\bullet}$, [Mel − H]$^{−}$, and [Mel + H]$^{+}$, making it difficult to make comparisons in this spectral region.

Melatonin Radical Cation, Mel$^{+\bullet}$ Bond lengths of C23–O30, C23–N22 (amide group), C6–O15, and C16–O15 (methoxy group) for neutral melatonin and all the ionic species for which IRMPD spectra were obtained from the minimum energy isomers calculated at the B3LYP/LACVP++** level of theory are listed in Table 2. The minimum energy structure of Mel$^{+\bullet}$ is shown in Figure 3(a). In comparison to neutral Mel, the C23–O30 bond length in Mel$^{+\bullet}$ is slightly longer whereas C23–N22 is marginally shorter. The C6–O15 bond distance is 1.37 Å for Mel and 1.32 Å in Mel$^{+\bullet}$, which is closer to the value of a C=O double bond. The O15–C16 bond length in Mel$^{+\bullet}$ is 1.45 Å, whereas that in Mel is 1.42 Å. The shortening of the C6–O15 bond and concurrent increase in O15–C16 bond length can be attributed to enhanced electron delocalization in Mel$^{+\bullet}$ compared to Mel.

A comparison of the measured spectrum of Mel$^{+\bullet}$ and the calculated spectrum of the minimum energy conformer is shown in Figure 3(a). The calculated frequencies are generally consistent with the experimental spectrum although there are noticeable differences. The match between the experimental and calculated spectra is not better for higher energy structures. The calculated amide I band is only 5 cm^{-1} to the red of the measured one at 1678 cm^{-1}. The calculated band for the indole N–H in plane bend occurs at 1575 cm^{-1}, shifted to the blue of the band in the experimental spectrum by 20 cm^{-1}. The width of the band in the experimental spectrum peaking at 1474 cm^{-1} suggests it could have contributions from two vibrations close in energy. The calculated spectrum predicts the amide II band at 1517 cm^{-1} and symmetric bend of the methoxy hydrogens at 1481 cm^{-1}. The calculated band at 1434 cm^{-1} lies only 10 cm^{-1} to the blue of the experimental band at 1424 cm^{-1} and can be attributed to the coupling of the methoxy hydrogen symmetric bend to the indole CH in plane bend motions. The calculated band at 1374 cm^{-1}, which lies only 9 cm^{-1} to the blue of the

Table 1. Absorption Band Maxima in cm^{-1} Observed in the Spectra of Mel$^{+\bullet}$, [Mel − H]$^-$ and [Mel + H]$^+$

Mel$^{+\bullet}$	[Mel − H]$^-$	[Mel + H]$^+$
1678	1678	1600–1800
1557	1575	1575
1474	1491	1478
1425	Weak absorption	1438
1366	–	1366
1327	1327	1317
1299	–	1290
1259	Weak absorption	1259

Each row groups bands in the spectra of the three ions that likely arise from similar structural motifs. Missing bands are indicated with a dashed line. In case of [Mel + H]$^+$, multiple overlapping absorptions are observed in the range in the first row

measured band in this region, occurs due to a combination of indole N1–H10 and C–H, methylene C–H$_2$, methoxy C–H$_3$ bends, and C15–O6 stretch. There are multiple absorptions in the region between 1200 and 1345 cm^{-1}. The calculated spectrum predicts several intense absorptions that are energetically close and hence only show up as a single band in the calculated spectrum upon convolution. Absorption in this region can be attributed to methylene C–H$_2$ and indole C5–H12 bends and the shoulder to the red of this band can be attributed to the amide III vibration, which is combination of N22–H29 in plane bending with C23–N22 stretch. The bands between 900 and 1200 cm^{-1} are mostly C–H and N–H in plane bend motions coupled to C–C stretches. Of particular interest is the relatively broad and weak feature at 970 cm^{-1} which matches quite well with the calculated band. This band is due to the excitation of the methoxy C16–O15 stretch. This stretch appears at 1235 cm^{-1} in the calculated spectrum of neutral Mel. The redshift in the band position is consistent with the increase in the C16–O15 bond length upon formation of the radical cation. The bands below 900 cm^{-1} can be attributed to ring deformation modes and indole C–H out of plane bend.

Deprotonated Melatonin, [Mel − H]$^-$ The two possible sites in Mel at which proton loss is likely to occur are the amide-N (N22) and the indole-N (N1). The minimum energy conformer for deprotonation at amide-N is 58.6 kJ/ mol higher in energy than its indole-N counterpart. Therefore, the structure

corresponding to deprotonation at indole is used for comparison with the experimental spectrum of [Mel − H]$^-$ (Figure 3(b)). The amide I band is easily identified at 1678 cm^{-1} in both computed and experimental spectra. A weak absorption is observed in the experimental spectrum at 1573 cm^{-1}. The closest match in the calculated spectrum is the band at 1600 cm^{-1} that is due to the coupled indole in plane C–C stretches and C–H bend motions. The amide II band is observed experimentally at 1491 and at 1531 cm^{-1} in the calculated spectrum. There are several vibrations that contribute to the broad shoulder to the red of the amide II band. From a comparison with the calculated spectrum, this band can be attributed to C–H bend motions of the amide methyl (C24), methylene, indole, and methoxy groups. The sharp band at 1328 cm^{-1} in the measured spectrum matches with the calculated band at 1350 cm^{-1} corresponding to coupled C–H bend motions of the different units in the [Mel − H]$^-$ ion. The amide III vibration is calculated to appear at 1275 cm^{-1}, which is in good agreement with the peak at 1250 cm^{-1} in the experimental spectrum. The methoxy O–C stretch is at 1213 cm^{-1} in the calculated spectrum and matches well the broad feature at the same frequency in the measured spectrum. This band has some contribution from coupling of the amide N22–H bend and methylene C–H$_2$ bend. The calculated band at 1165 cm^{-1} arises due to the C2–H bend coupled with the methylene C–H$_2$ bend motions and matches the experimental band at 1151 cm^{-1}. The bands below 1100 cm^{-1} can be attributed to ring deformation modes coupled to C–H bends and the bands further to the red

Table 2. Bond Lengths, in Angstrom, of the C23–O30, C23–N22, C6–O15, and C16–O15, for Neutral Melatonin and All the Ionic Species and Complexes as Obtained from the Energy Minimized Geometries at the B3LYP/LACVP++** Level of Theory

Bonds	Mel	Mel$^+$	[Mel-H]$^-$	[Mel+H]$^+$	[Mel-Li]$^+$	[Mel-Na]$^+$	[Mel-K]$^+$	[Mel-Ca]$^{2+}$	[Mel-Sr]$^{2+}$	[(Mel-H) + Mg]$^+$
C23–O30	1.23	1.24	1.24	1.24	1.26	1.25	1.25	1.28	1.27	1.31
					1.25	1.25	1.25	1.27	1.27	1.31
C23–N22	1.37	1.36	1.35	1.36	1.34	1.35	1.35	1.33	1.33	1.32
					1.34	1.35	1.35	1.33	1.33	1.32
C6–O15	1.37	1.32	1.40	1.32	1.41	1.40	1.40	1.42	1.42	1.42
					1.36	1.36	1.37	1.35	1.35	1.35
C16–O15	1.42	1.45	1.41	1.45	1.45	1.44	1.44	1.47	1.47	1.45
					1.43	1.43	1.43	1.45	1.45	1.44

For [Mel + H]$^+$, the bond lengths are of isomer **4c**. For the metal complexes, the first row corresponds to the binding motif **1** (shaded in light blue) and the second row to binding motif **2**. See text and Figures 4 and 5 for more details. For [(Mel − H) + Mg]$^+$, the bond lengths shown are for conformers **6a** (highlighted in gray) and **b** (Figure 6)
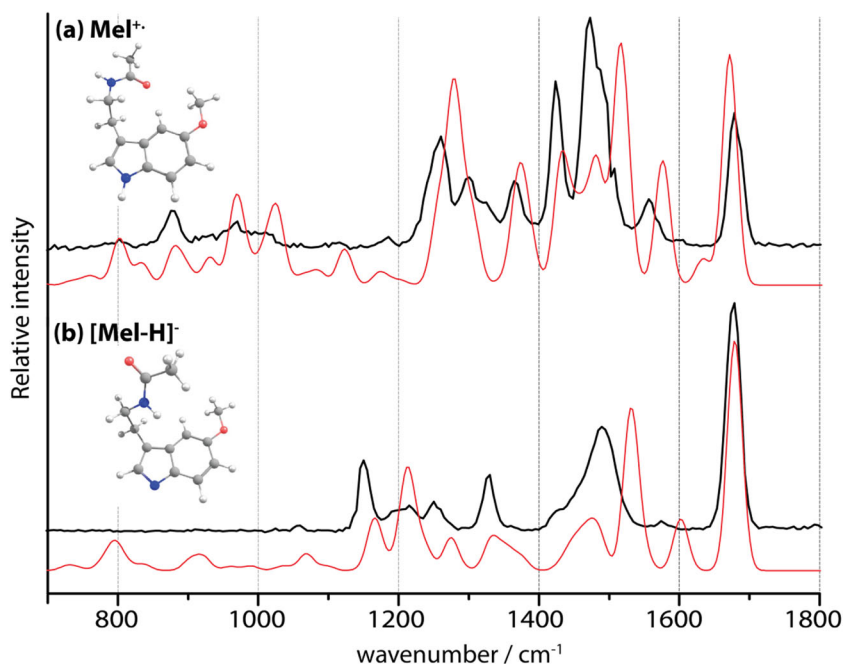
Figure 3. Comparison of IRMPD spectra (black trace) with calculated spectra of their lowest energy conformers (red trace) of (**a**) Mel$^{+\bullet}$ and (**b**) [Mel − H]$^-$. The corresponding structures are inset

around 800 cm^{-1} are out of plane C–H bends which are too weak to be observed clearly in the experimental spectrum.

The appearance of the methoxy stretch at 1213 cm^{-1} in the spectrum of [Mel − H]$^-$, as opposed to 970 cm^{-1} in Mel$^{+\bullet}$, is also consistent with the shortening of the C16–O15 bond in [Mel − H]$^-$ (Table 2). Also of note is the enhanced intensity of the C2–H11 bend at 1165 cm^{-1} in the spectrum of [Mel − H]$^-$ compared to Mel$^{+\bullet}$. This enhancement can be attributed to a greater change in dipole moment on account of proximity to the charge center in the molecule.

Protonated Melatonin, [Mel + H]$^+$ Several isomers of protonated melatonin are possible owing to multiple energetically competitive sites that can accommodate an excess proton (Figure 1). Figure 4 shows the structures of the most stable conformers for the five lowest energy isomers of [Mel + H]$^+$, their relative Gibbs free energies, and a comparison of the corresponding calculated spectra (red trace) with respect to the experimental spectrum (black trace). A previous gas phase study on protonated melatonin identified protonation at C5 as the lowest energy isomer, which is consistent with our calculations (**4a**) [27]. There are three additional isomers (**4b-d**) within 10 kJ/ mol of **4a** in which the proton is bound to a carbon atom of the indole group due to favorable charge delocalization. **4e** corresponds to protonation at the carbonyl oxygen of the amide group and is 13.6 kJ/ mol higher in energy than **4a**. A visual inspection reveals that the calculated spectrum for **4c** provides the best match with the experimental spectrum, although this structure is computed to be 6.9 kJ/mol higher in energy than **4a**.

There are several overlapping absorptions in the measured spectrum of [Mel + H]$^+$ between 1540 and 1750 cm^{-1}. The feature with the highest intensity is at 1616 cm^{-1}, which is

redshifted from the position of the amide I stretch as observed in the spectra of Mel$^{+\bullet}$ and [Mel − H]$^-$. The shift suggests that the amide carbonyl group undergoes an additional interaction in [Mel + H]$^+$ absent in Mel$^{+\bullet}$ and [Mel − H]$^-$. There is a band at 1693 cm^{-1} that is about one third as intense as the band at 1616 cm^{-1}. Although the band position is within 15 cm^{-1} of the computed amide I stretch, the relative intensity is weaker than that of the computed band. The amide I stretch in the calculated spectrum of **4c** is centered at 1690 cm^{-1} and is the most intense band in the spectrum. The calculated spectrum of isomer **4c** further predicts three bands at 1564, 1617, and 1638 cm^{-1}. The latter two are smeared out in the calculated spectra due to the convolution. All three are combinations of indole ring distortion modes with indole-N-H in plane bend vibration. This region in the spectra of Mel$^{+\bullet}$ and [Mel − H]$^-$ has absorptions attributed to indole C–H distortions, and the N1–H bend occurs at 1557 cm^{-1} in the spectrum of Mel$^{+\bullet}$. The large blue shift in the frequency of the N–H bend in the spectrum of [Mel + H]$^+$ can be attributed to N1 having a partial positive charge in **4c**. The charge could also play a role in enhancing the absorption intensities as changes in dipole moments associated with these vibrations are likely to be greater. The shoulders at 1589 and 1651 cm^{-1} could then be attributed to the calculated bands at 1564 and 1638 cm^{-1}, whose calculated intensities are likely underestimated. However, this does not explain the lower than expected intensity of the amide I band. It is possible that the harmonic calculations presented here do not capture a coupling of the amide I stretch with one of the indole ring distortion modes, which could result in change in the expected intensities and absorption position of the amide I band. Anharmonic calculations could provide a more detailed picture of the coupling mechanisms in this isomer.
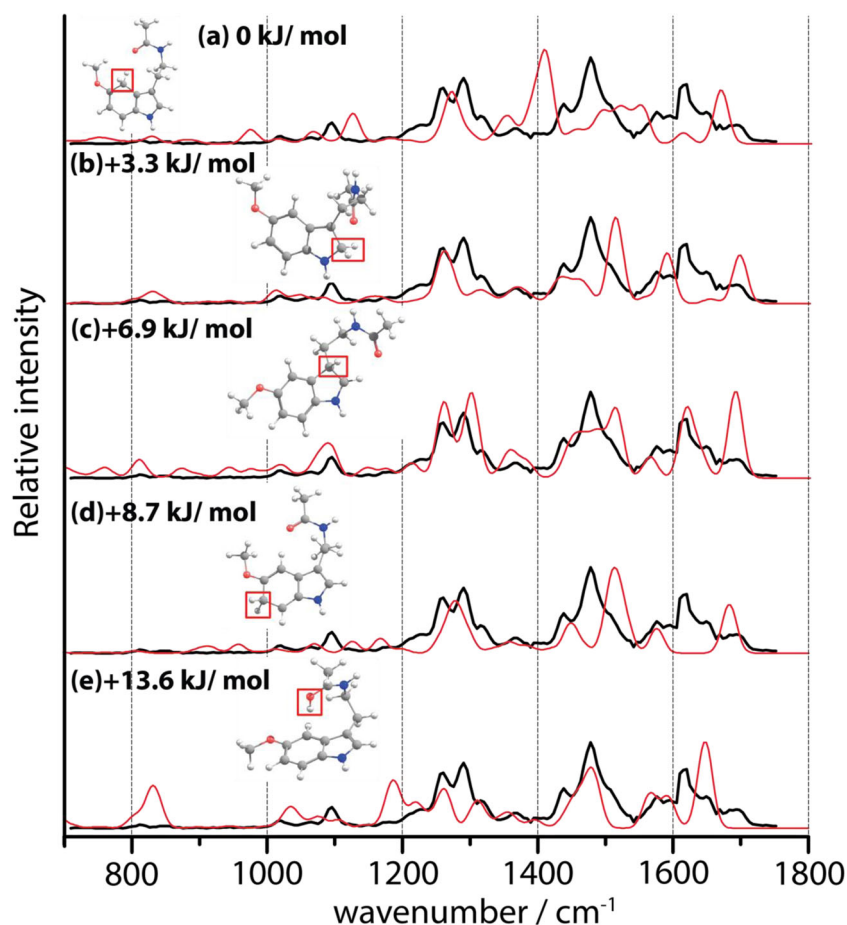
Figure 4. Comparison of the IRMPD spectrum of [Mel + H]$^+$ (black trace) with calculated spectra (red trace) for five of the lowest energy conformers. Isomer **4(a)** is protonated at C5, **4(b)** at C2, **4(c)** at C3, **4(d)** at C7, and **4(e)** at O30

The correlation between experimental and calculated bands of **4c** below 1540 cm^{-1} is more straightforward. The peak at 1478 cm^{-1} is the amide II stretch and the shoulder at 1440 cm^{-1} arises from nearby bending motions of hydrogen atoms of the methoxy group, C20, C21, and C24, and indole ring distortion. The weak band centered at 1365 cm^{-1} arises from bends of the hydrogen atoms of C20, C21, and C24 atoms. The broad feature between 1158 and 1342 cm^{-1} contains contributions from in plane C–H bend motions of the indole ring centered at 1292 cm^{-1} and the amide III stretch at 1257 cm^{-1}. The shoulder that appears to the red of this band and the absorption at 1095 cm^{-1} can be attributed to the bending motions of the additional hydrogen at C3 coupled to indole, methylene, and amide H bends. The calculated spectra of the isomers other than **4c** have absorption bands around 1100 cm^{-1}, which arise from indole C–H bend motions coupled to indole C–C stretches and also C24–H bend motions in the amide side chain. In all the isomers except **4a**, these absorptions are weak. The band at 1126 cm^{-1} in the calculated spectrum of isomer **4a** arises due to indole C–H and N–H in plane bends. Therefore, none of the isomers except **4c** have contributions from the extra H in this region of the spectrum. This band at 1095 cm^{-1} is also absent in the experimental spectra of Mel$^{+•}$ and [Mel − H]$^-$ indicating the absence of the additional proton in these two

ions. Based on the overall good agreement between experiment and theory for isomer **4c**, C3 appears to be the dominant protonation site in melatonin. However, given the small differences in the relative energies of the isomers, it is possible that some of the other isomers may provide a small contribution to the measured spectrum as well.

Protonation at methoxy-O, amide-N, and indole-N results in isomers with relative Gibbs free energies greater than 60 kJ/mol with respect to protonation at C3 and therefore have not been discussed. Reduced charge delocalization upon protonation at these sites is the most likely reason why these sites are not favorable for protonation.

Spectra of Melatonin Metal Complexes

Structures of [Mel + M]$^+$ (M = Li, Na, K) Spectra for complexes of melatonin with Li$^+$, Na$^+$, and K$^+$ (**5a-c**) are shown in Figure 5. Also shown are calculated spectra of two conformers, labeled 1 (blue traces) and 2 (red traces) for all three metal complexes. The binding motifs of the metal ions in conformers **1** and **2** are shown in **5a** for Li$^+$ complexation. The same motifs have been identified for complexation of Mel with all other metal ions in this study, except for Mg^{2+}. In conformer
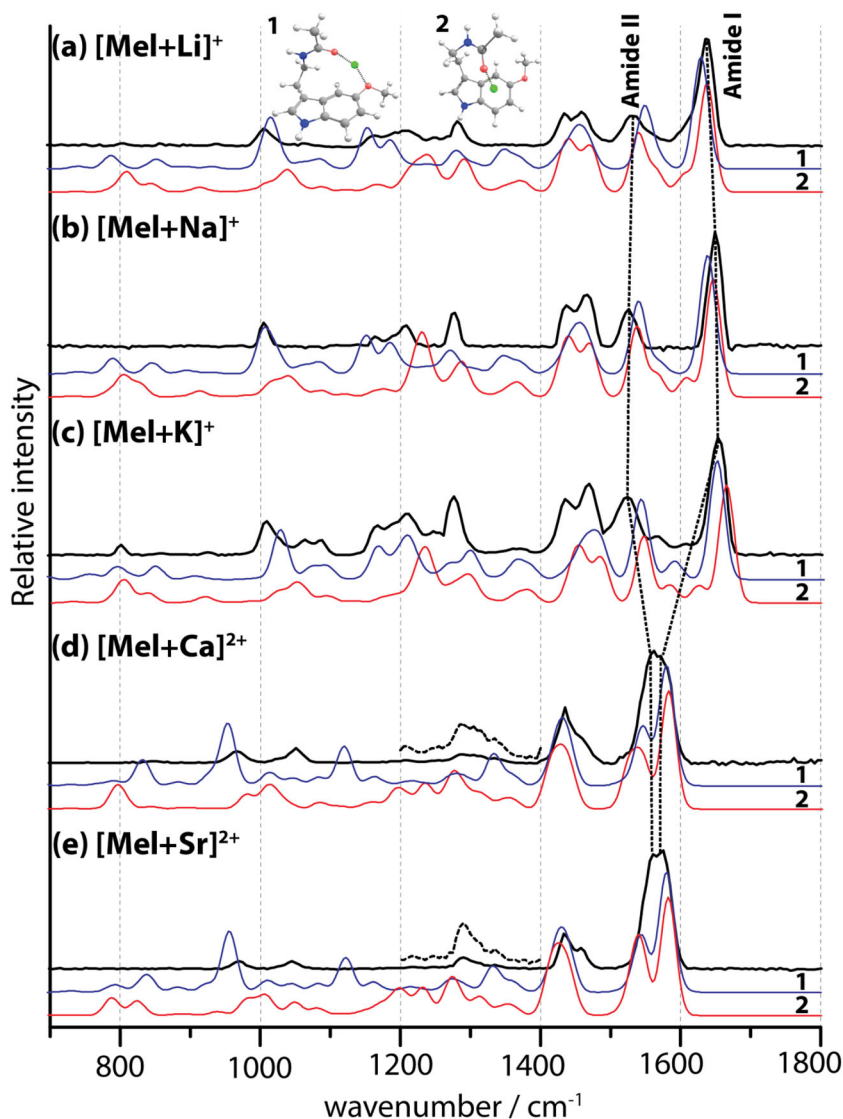
Figure 5. The spectra of [Mel + M]$^{z+}$, where M = (**a**) Li$^+$, (**b**) Na$^+$, (**c**) K$^+$, (**d**) Ca^{2+}, and (**e**) Sr^{2+}. The experimental spectra are in black. Two conformers with different binding interactions are compared: **1** corresponds to binding through the amide-O30 and methoxy-O15 and **2** corresponds to binding through amide-O30 and π-electron cloud of the indole unit. These two interactions are shown for the [Mel + Li]$^+$ complex. The corresponding calculated spectra for **1** and **2** are shown in blue and red traces, respectively, for all the [Mel + M]$^{z+}$ complexes. Also shown are the amide I and II bands and the shifts in their absorption frequencies with the coordinating metal ions. The dashed traces above the spectra of [Mel + Ca]$^{2+}$ and [Mel + Sr]$^{2+}$ are ×3 magnification of the region between 1200 and 1400 cm^{-1}

1, the metal ion is coordinated to the amide-O30 and the methoxy-O15. This motif is the lowest energy conformer. In conformer **2**, the metal ion interacts with the π-electron cloud of the indole group and with the amide oxygen atom. There is no interaction with the methoxy-O in this conformer. The relative Gibbs free energies of the conformers **2** compared to conformers **1** are 22.4, 19.0, and 21.2 kJ/ mol for the Li$^+$, Na$^+$, and K$^+$ complexes, respectively. The relevant bond lengths for conformers **1** and **2** are given in Table 2. The C6–O15 bond length is predicted to increase with increasing metal ion size in conformer **1**, whereas in conformer **2**, this bond length shows the opposite trend. Vibrations associated with this bond are expected to display a red shift should the metal ions bind with

Mel as in conformer **1** and should serve as a marker to distinguish between the two predicted binding motifs. In comparison, the C16–O15 bond length decreases with increasing size of the metal ion for both conformers.

The band at around 1650 cm^{-1} is the most intense for all three ion complexes. This is the amide I vibration and the calculated band for both conformers **1** and **2** match the measured band. Compared to [Mel + Li]$^+$, the amide I band is blue shifted by 10 cm^{-1} for [Mel + Na]$^+$ and a further 15 cm^{-1} for [Mel + K]$^+$. The blue shift indicates the interaction of the metal ions with Mel weakens with increasing size of the ion. The decrease in the calculated C23–O30 bond length with increasing size of the metal ion (Table 2) is further evidence of

weakening interaction of Mel with the metal ion as the size of the latter increases. The amide I band has a shoulder to the red for [Mel + Li]$^+$ at ~ 1607 cm^{-1}, which is absent for complexation with Na$^+$ and is relatively weak for the K$^+$ complex (~ 1625 cm^{-1}). The calculated spectra for both conformers **1** and **2** have weak bands that can be assigned to indole ring distortion modes between 1605 and 1625 cm^{-1}. The relative intensity of the indole ring distortion is greater in conformer **2** because of the interaction of the π-electron cloud with the metal ion. The band at around 1530 cm^{-1} is the amide II vibration and is predicted for both conformers **1** and **2**. The absorption maximum of the amide II band undergoes a redshift of 8 cm^{-1} in [Mel + Na]$^+$ from [Mel + Li]$^+$, and only 3 cm^{-1} in [Mel + K]$^+$ compared to [Mel + Na]$^+$, indicating lengthening of the amide N–H and the C23–N22 bond lengths consistent with the calculated bond lengths of both conformers **1** and **2** (Table 1). The amide II bands have weak shoulders to the blue arising from indole C–C bends coupled to indole C–H bends.

The experimental spectra have two overlapping bands between 1400 and 1500 cm^{-1} for the three alkali metal ion-Mel complexes. These bands can be attributed from the computations to C–H bend motions of the methoxy, indole, methylene, and the amide groups. The methoxy symmetric C–H bend motions and the C15–O6 stretch coupled to the indole C–H bends occur at slightly higher energies (~ 1465 cm^{-1}). Therefore, the peak at the higher frequency can be attributed to this vibration. This peak blue shifts with increasing alkali metal ion size (7 cm^{-1} from [Mel + Li]$^+$ to [Mel + Na]$^+$ and 3 cm^{-1} from [Mel + Na]$^+$ to [Mel + K]$^+$) indicating a decreasing interaction between the ion and the methoxy oxygen with increasing cation size. This blue shift is consistent with the binding motif of conformer **1**. The calculated spectra of conformers **1** do not show the semi-resolved bands as in the experimental spectrum due to their predicted positions being closer, which causes the convolution to merge the individual bands. The low frequency band at 1436 cm^{-1} undergoes virtually no shift in its position, indicating that this band is not due to a binding motif involved in interaction with the metal ion. This is consistent with the fact that these bands are primarily C–H bend motions of the indole, amide, methoxy, and methylene groups and none of these interact with the metal ion in conformer **1**.

The bands at ~ 1360 cm^{-1} that appear in the calculated spectra of both conformers **1** and **2** show up only with very weak intensity in the spectrum of [Mel + K]$^+$. These are the C24–H bend motions of the amide methyl group and the methylene groups and are probably too weak to be detected in the spectra of [Mel + Li]$^+$ and [Mel + Na]$^+$.

There is a slight redshift in the band at around 1280 cm^{-1} going from [Mel + Li]$^+$ to [Mel + K]$^+$. This band arises due to methylene C–H$_2$ bend motions. This is most likely induced by the proximity of the methylene groups to the metal ion. There is a weak absorption to the red of this band near ~ 1250 cm^{-1}, due to coupled bends of the methylene C–H$_2$, amide C24–H, and indole ring distortion. The intensity of this band is the weakest for [Mel + Na]$^+$ but the band position appears to remain unaffected by the complexing metal ion. The subsequent bands

to the red are broad and are also unaffected in their position by the metal ion. These are attributed to various coupled C–H bend vibrations. A prominent band at 1006 cm^{-1} is primarily due to the excitation of the C5–H12 bend motion. To the blue of this band lies a broad feature, centered at 1070 cm^{-1} in the spectrum of [Mel + K]$^+$, and it is also observed for [Mel + Li]$^+$ with weaker intensity. This feature is hardly discernible for [Mel + Na]$^+$ due to the weak intensity. This band is attributed to indole C–H and N–H bends, methylene C–H$_2$ and amide C24–H bends, and C–C and C–N (C21 and C23) bends in the methylene and the amide units.

Although the calculated spectra for conformers **2** for all three metal complexes show decent matches with the experimental spectra between 1400 and 1700 cm^{-1}, conformers **1** provide a better match between 1100 and 1400 cm^{-1}. Further, conformers **2** are more than 19 kJ/mol higher in energy than conformers **1** indicating the latter are the most likely structures of alkali metal ion-Mel complexes.

Structures of [Mel + M]$^{2+}$ (M = Ca, Sr) There are two possible binding motifs for Ca^{2+} and Sr^{2+} to Mel that are similar to the Mel complexes with alkali metal ions. A comparison of the measured spectra with calculated spectra for the two conformers is shown in Figure 5(d), (e). The spectrum of [Mel + Sr]$^{2+}$ is very similar to that of [Mel + Ca]$^{2+}$, which suggests that the binding motifs are the same for these ions. The calculated spectra of conformers **1** and **2** are also very similar for these two conformers. Therefore, the discussion is limited to [Mel + Ca]$^{2+}$ complex as the same arguments can be extended to [Mel + Sr]$^{2+}$. Conformer **1**, in which Ca^{2+} interacts with amide-O30 and methoxy-O15, is 35.5 kJ/ mol (18 kJ/ mol) lower in energy than conformer **2**, in which the Ca^{2+} ion is shared between the amide-O and the aromatic ring. The higher free energy makes it unlikely that conformer **2** is present in any significant quantity in the ion ensemble probed in the experiment.

The amide I band at 1569 cm^{-1} is shifted to the red with respect to the alkali metal complexes, induced by interaction with + 2 charge, whereas the amide II band shows a blue shift. Hence, these bands overlap in the measured spectrum and the width of the observed band is greater than either of the individual amide I and amide II bands in the spectra of the alkali metal ions. Similar trends in the absorption frequencies of the amide I and II band have also been reported for di- and trialanine complexes of alkali and alkaline earth metal ions [26]. The differences between the band positions of the amide I and II bands decrease with higher charge density of the metal ion, from ~ 180 cm^{-1} in the K$^+$ complex with trialanine to ~ 30 cm^{-1} in the Ca^{2+} complex [26]. The band at 1435 cm^{-1} in the spectrum of [Mel + Ca]$^{2+}$ can be attributed to C24–H bend motions of the amide methyl and methylene units. The shoulder to the blue of this peak arises due to the coupling of C24–H bend motions of the amide and methylene groups with those of the indole and methoxy groups. In the calculated spectrum of conformer **1**, this band appears 3 cm^{-1} to the red. The broad

feature peaking at 1292 cm^{-1} arises due to C–H bend motions of the indole, methylene, and amide units as well as amide III stretch. A comparison of the calculated spectra of the two conformers considered here reveals only marginal differences with respect to the measured spectrum between 1150 and 1700 cm^{-1}. There is some ambiguity regarding the assignment of the broad experimental bands observed between 1150 and 1385 cm^{-1}. Conformer **1** shows two clear peaks at 1334 and 1278 cm^{-1} which can be assigned to the measured peaks at 1338 and 1292 cm^{-1}, respectively (dashed traces in Figure 5(d), (e)). The peak at 1334 cm^{-1} results from a coupling of the indole ring distortion mode with methylene C–H$_2$ bend motions, whereas the peak at 1278 cm^{-1} can be attributed to coupling of indole C–H in plane, methylene C–H$_2$, and amide N–H bend motions. The multiple bands that occur between 1060 and 1390 cm^{-1} in the calculated spectrum of conformer **2** arise from various combinations of indole C–H in plane, methylene C–H$_2$, amide N22–H, amide C–H, methoxy C–H$_3$ bends, indole ring distortion, and O15–C6 stretches. These bending motions have more intensity in the calculated spectrum of conformer **2** than conformer **1** likely because the proximity of the Ca^{2+} ion to the indole unit induces a greater change in dipole moment.

The major differences between the calculated spectra arise between 900 and 1150 cm^{-1} where the methoxy O15–C16 stretch is predicted to occur. The experimental spectrum has two bands at 967 and 1051 cm^{-1}. The separation between these two bands is 83 cm^{-1}. Neither conformer **1** nor conformer **2** has a pair of bands that match this separation. The band at 954 cm^{-1} in the calculated spectrum of conformer **1** is attributed to the O15–C16 stretch, whereas the calculated band at 1120 cm^{-1} arises from excitation of C–H bend vibrations of the methoxy and indole units. This band can be tentatively assigned to the band at 1051 cm^{-1} in the measured spectrum. The relative intensities of these bands in conformer **1** are high due to the interaction of the methoxy-O with the Ca^{2+} ion. The calculated spectrum of conformer **2** has two overlapping bands with peaks at 982 and 1015 cm^{-1}, which could also be potentially assigned to the measured bands. The peak at 982 cm^{-1} can be assigned to the O15–C16 stretch coupled to indole C–H bends and the peak at 1015 cm^{-1} arises from C–H bend motions of indole, methylene, and amide C24–H units. The weak and broad band at 846 cm^{-1} in the experimental spectrum results from out of plane indole C–H bends and are also reported in the calculated spectra of conformers **1** and **2**. Based on the above spectral comparisons, it is difficult to make an unambiguous structural assignment. However, based on the high relative free energy of conformer **2** and the fact that the charge density in neutral melatonin is highest at the methoxy-O, it is likely that the structures of these ions is closest to conformer **1**.

The Structure of [(Mel – H) + Mg]$^+$ A comparison of the measured spectrum (black trace) of [(Mel – H) + Mg]$^+$ with calculated spectra (red traces) of two conformers, where the deprotonation site is the amide-N, is shown in Figure 6(a), (b).

The structure of the lowest energy conformer in which the indole-N is deprotonated is shown in 6(c) and its relative free energy is 65.7 kJ/ mol higher than conformer 6(a). This is in contrast to [Mel – H]$^-$, where the favored deprotonation site is the indole-N. In conformer **6a**, the Mg^{2+} interacts with the amide-O and the C5 atom but not the π-electron cloud of the indole ring. The electron density at this carbon atom is enhanced by delocalization of the oxygen lone pair from the methoxy group. This is apparent from a O15–C6 bond length of 1.35 Å relative to 1.37 Å in Mel (Table 2). The H12 atom attached to the C5 atom is bent 21° below the plane of the aromatic ring, indicating the loss of sp^2 character of the C5 atom due to interaction with Mg^{2+}. In the conformer **6b**, which is 7.6 kJ/ mol higher in energy, the Mg^{2+} interacts with the methoxy-O, resulting in the 15O atom being located above the plane of the aromatic ring and the O15–C6 bond length is 1.42 Å. The displacement of the oxygen atom out of the plane of the aromatic ring leads to loss of delocalization and hence the higher energy of this conformer.

The amide I band at 1525 cm^{-1} is significantly to the red of the corresponding bands in the spectra of the other metal ion complexes of melatonin due to the deprotonated amide-N. This band is wider by almost 10 cm^{-1} compared to the amide I bands in the spectra of Mel-alkali metal complexes, Mel$^{+\bullet}$ and [Mel – H]$^-$, owing to the overlap with the indole ring distortion modes. The amide II vibration is absent in the spectrum of this complex due to deprotonation at amide-N22. Three partially resolved bands occur between 1365 and 1491 cm^{-1}. These features are also observed in the calculated spectrum of isomer **6a**, shifted to lower frequencies and with different relative intensities. The first two features are predicted at frequencies lower by about 22 cm^{-1}, whereas the third feature is ~ 14 cm^{-1} lower in energy in the calculated spectrum. The band at 1341 cm^{-1} occurs due to excitation of the methylene C–H$_2$ bends coupled with the indole C–H and amide C24–H bends. This band is calculated to be at 1320 cm^{-1}. The calculated band at 1286 cm^{-1} shows excellent agreement with the experimental band at 1286 cm^{-1} and is attributed to the indole ring distortion modes coupled to in plane C–H and N–H bends, methoxy C–H$_3$ bends, and O15–C6 bend motions. Further coupled modes of in-plane C–H bends are predicted between 1100 and 1260 cm^{-1}. There are several weak and broad bands below 1100 cm^{-1}, along with two well discernible features at 1048 and 992 cm^{-1}. The former can be attributed to C–H bends of the methylene and indole groups coupled with ring distortion modes. The measured band at 992 cm^{-1} corresponds well to the calculated band at the same frequency and occurs due to out of plane bend of the H12 atom coupled to ring distortion modes and asymmetric bend of the H atoms of the amide methyl group. The calculated spectrum also predicts the in-plane bend of the H12 atom along with multiple concerted indole C–H bend motions to occur at around 800 cm^{-1}. Weak and broad absorptions are observed between 750 and 900 cm^{-1} in the measured spectrum.

The amide I band of the calculated spectrum of conformer **6b** is shifted to the red of the experimental band by ~ 28 cm^{-1}. The region between 1100 and 1468 cm^{-1} in the calculated

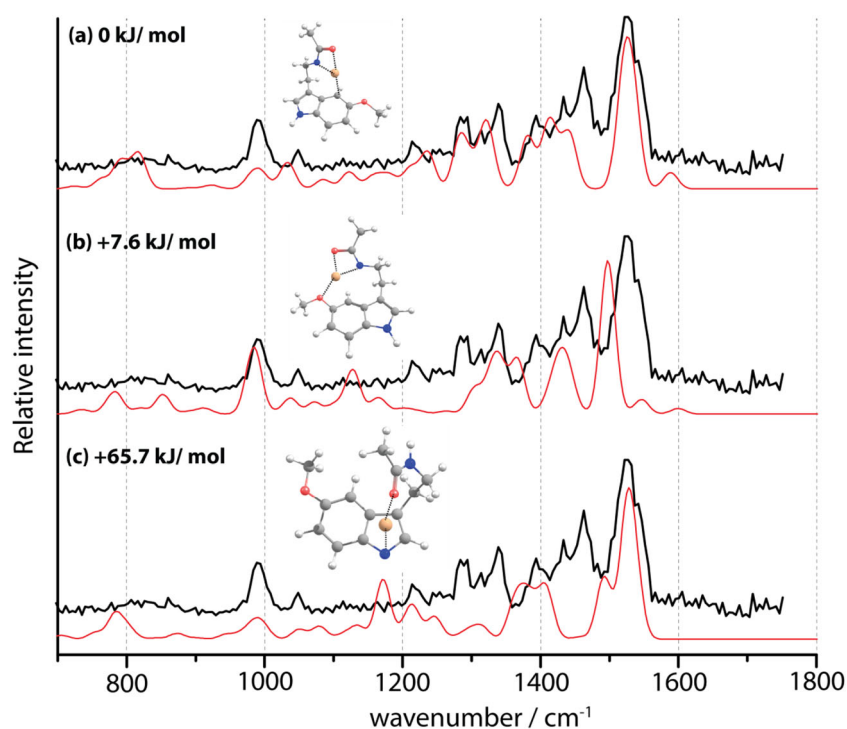**Figure 6.** Comparison of the IRMPD spectrum (black trace) of $[(Mel - H) + Mg]^+$ with calculated spectra (red trace). Conformers **6(a)** and **6(b)** correspond to deprotonation at amide-N and **6(c)** represents the lowest energy conformer for deprotonation at indole-N

spectrum shows a band profile that is quite different from the measured spectrum. A decent match is, however, observed for the experimental bands at 1048 and 992 cm^{-1}. The intense band at 984 cm^{-1} in the calculated spectrum arises from a combination of indole C–H bends and methoxy C6–O15 stretch. The weaker band at 1033 cm^{-1} in the calculated spectrum is due to a combination of indole C–H, N–H and methylene C–H_2 bend motions. Given the mismatch of the other calculated bands with the measured spectrum, it is likely that the similarities for the two bands at 1048 and 992 cm^{-1} are accidental. For isomer **6c**, only the amide I band provides a good match between the measured and the experimental spectra. The amide II band at 1490 cm^{-1} appears as a shoulder to the amide I band in the calculated spectrum and contributes to the widening of the band. Although the resultant width is comparable to the experimental band, none of the other bands below 1452 cm^{-1} show agreement with the calculated spectrum of **6c**. The dissimilarities between the measured spectrum of $[(Mel - H) + Mg]^+$ and the calculated spectrum of isomer **6c** and its high relative free energy clearly indicate that Mel is deprotonated at the amide-N when complexed with Mg^{2+}.

The preference of Mg^{2+} to bind to the amide-N by displacing the proton is consistent with earlier gas phase studies on metal ion interaction with peptides. IRMPD spectra of complexes of the dipeptide PhePhe with Mg^{2+} show clear evidence of the metal ion inducing an iminol tautomerization to bind to the deprotonated amide-N [35]. The spectrum is characterized by the absence of the amide II band. In case of Mel, however, the proton is not retained and the metal also interacts with the amide-O. The iminol binding motif has also

been observed for transition metal ions in their complexes with peptides and has been characterized by IRMPD spectroscopy and quantum chemical calculations [19, 36].

Conclusion

Despite the large volume of work that has characterized the interactions of melatonin with metal ions in solution, the exact nature of these interactions remains unknown. The present studies report on the binding interactions of melatonin with alkali and alkaline earth metal ions in the gas phase. All the metal ions except Mg^{2+} are found to bind preferentially with the O30 and the O15 attached to the amide and the methoxy groups, respectively. Although, higher in energy, isomers in which the metal ion interacts with the aromatic π ring could also be present under the experimental conditions. The high energy conformers could potentially result from kinetic trapping after electrospray ionization [37]. The metal ion dependent frequency shifts of the amide I and II bands are small for the alkali metal ions but the trends are consistent with the extent of interaction of melatonin with the individual metal ions. The blue shift of the amide I band and the red shift of the amide II band with increasing ionic radii are also consistent with literature data on polypeptide complexes with metal ions [26]. Mel is deprotonated at the amide-N with Mg^{2+} and the metal ion coordinates to the amide center (N22 and O30). This is similar to iminol tautomerization observed in dipeptides when bound to Mg^{2+} [35]. Reports from solution phase studies claim that

the interaction of melatonin with Ca^{2+} is not favorable. However, we do in fact observe this complex in the gas phase. This disparity likely arises from the competitive interactions between the ion and water molecules that influence binding. It would be interesting to investigate the chemistry of hydrated metal complexes of melatonin to shed light on the role of water molecules on the stability of Mel-metal ion complexes as has been done for other gaseous ions [38–40].

IRMPD spectra have been measured for cationic, deprotonated and protonated melatonin. As melatonin undergoes redox reactions, it is possible that these species appear as reaction intermediates. The electron is lost from the methoxy-O to form $Mel^{+\bullet}$, whereas the hydrogen is lost from the indole-N to generate $[Mel - H]^-$. The assignment of the site of protonation was more ambiguous, with multiple isomers likely being present in the probed ion population. The calculated spectrum of the isomer with the proton at C3 of the indole group provides the closest match with the experimental spectrum, even though energetically, the most favored protonation site is at C5 of the indole group.

The results reported here are the first gas phase spectroscopic studies of melatonin ions and the interaction of neutral melatonin with metal ions. These spectra should provide benchmarks for further detailed theoretical characterization of non-covalent interactions in these complexes and possibly understand their role in the biochemistry of melatonin in living organisms.

Acknowledgements

References

1. Sugden, D.: Melatonin biosynthesis in the mammalian pineal-gland. Experientia. **45**, 922–932 (1989)

2. Hardeland, R., Pandi-Perumal, S.R., Cardinali, D.P.: Melatonin. Int. J. Biochem. Cell Biol. **38**, 313–316 (2006)

3. Cassone, V.M.: Melatonin's role in vertebrate circadian rhythms. Chronobiol. Int. **15**, 457–473 (1998)

4. Simko, F., Paulis, L.: Melatonin as a potential antihypertensive treatment. J. Pineal Res. **42**, 319–322 (2007)

5. Cardinali, D.P., Srinivasan, V., Brzezinski, A., Brown, G.M.: Melatonin and its analogs in insomnia and depression. J. Pineal Res. **52**, 365–375 (2012)

6. Zang, L.Y., Cosma, G., Gardner, H., Vallyathan, V.: Scavenging of reactive oxygen species by melatonin. Biochim. Biophys. Acta. **1425**, 469–477 (1998)

7. Reiter, R.J., Robinson, J.: Melatonin: Your Body's Natural Wonder Drug. Bantam Books, New York (1995)

8. Romero, A., Ramos, E., de Los Rios, C., Egea, J., del Pino, J., Reiter, R.J.: A review of metal-catalyzed molecular damage: protection by melatonin. J. Pineal Res. **56**, 343–370 (2014)

9. Lahiri, D.K., Chen, D., Lahiri, P., Rogers, J.T., Greig, N.H., Bondy, S.: Melatonin, metals, and gene expression: implications in aging and neurodegenerative disorders. Ann. N. Y. Acad. Sci. **1035**, 216–230 (2004)

10. Kabuto, H., Yokoi, I., Ogawa, N.: Melatonin inhibits iron-induced epileptic discharges in rats by suppressing peroxidation. Epilepsia. **39**, 237–243 (1998)

11. Lin, A.M., Ho, L.T.: Melatonin suppresses iron-induced neurodegeneration in rat brain. Free Radic. Biol. Med. **28**, 904–911 (2000)

12. Limson, J., Nyokong, T., Daya, S.: The interaction of melatonin and its precursors with aluminium, cadmium, copper, iron, lead, and zinc: an adsorptive voltammetric study. J. Pineal Res. **24**, 15–21 (1998)

13. Lack, B., Daya, S., Nyokong, T.: Interaction of serotonin and melatonin with sodium, potassium, calcium, lithium and aluminium. J. Pineal Res. **31**, 102–108 (2001)

14. Mocchegiani, E., Santarelli, L., Tibaldi, A., Muzzioli, M., Bulian, D., Cipriano, K., Olivieri, F., Fabris, N.: Presence of links between zinc and melatonin during the circadian cycle in old mice: effects on thymic endocrine activity and on the survival. J. Neuroimmunol. **86**, 111–122 (1998)

15. Prell, J.S., Demireva, M., Oomens, J., Williams, E.R.: Role of sequence in salt-bridge formation for alkali metal cationized GlyArg and ArgGly investigated with IRMPD spectroscopy and theory. J. Am. Chem. Soc. **131**, 1232–1242 (2009)

16. Dunbar, R.C., Oomens, J., Berden, G., Lau, J.K., Verkerk, U.H., Hopkinson, A.C., Siu, K.W.: Metal ion complexes with HisGly: comparison with PhePhe and PheGly. J. Phys. Chem. A. **117**, 5335–5343 (2013)

17. Dunbar, R.C., Berden, G., Martens, J.K., Oomens, J.: Divalent metal-ion complexes with dipeptide ligands having Phe and His side-chain anchors: effects of sequence, metal ion, and anchor. J. Phys. Chem. A. **119**, 9901–9909 (2015)

18. Bush, M.F., Oomens, J., Saykally, R.J., Williams, E.R.: Alkali metal ion binding to glutamine and glutamine derivatives investigated by infrared action spectroscopy and theory. J. Phys. Chem. A. **112**, 8578–8584 (2008)

19. Dunbar, R.C., Berden, G., Oomens, J.: How does a small peptide choose how to bind a metal ion? IRMPD and computational survey of CS versus Iminol binding preferences. Int. J. Mass Spectrom. **354**, 356–364 (2013)

20. Ruan, C.H., Yang, Z.B., Hallowita, N., Rodgers, M.T.: Cation-pi interactions with a model for the side chain of tryptophan: structures and absolute binding energies of alkali metal cation-indole complexes. J. Phys. Chem. A. **109**, 11539–11550 (2005)

21. Florio, G.M., Christie, R.A., Jordan, K.D., Zwier, T.S.: Conformational preferences of jet-cooled melatonin: probing trans- and cis-amide regions of the potential energy surface. J. Am. Chem. Soc. **124**, 10236–10247 (2002)

22. Yi, J.T., Brand, C., Wollenhaupt, M., Pratt, D.W., Leo Meerts, W., Schmitt, M.: Rotationally resolved electronic spectroscopy of biomolecules in the gas phase. Melatonin. J. Mol. Spectrosc. **268**, 115–122 (2011)

23. Bayari, S., Ide, S.: Fourier transform infrared spectra and molecular structure of 5-methoxytryptamine, N-acetyl-5-methoxytryptamine and N-phenylsulfonamide-5-methoxytryptamine. Spectrochim. Acta A Mol. Biomol. Spectrosc. **59**, 1255–1263 (2003)

24. Singh, G., Abbas, J.M., Dogra, S.D., Sachdeva, R., Rai, B., Tripathi, S.K., Prakash, S., Sathe, V., Saini, G.S.: Vibrational and electronic spectroscopic studies of melatonin. Spectrochim. Acta A Mol. Biomol. Spectrosc. **118**, 73–81 (2014)

25. Stein, S.E.: Infrared Spectra in NIST Chemistry WebBook. In: Mallard, W.G., Linstrom, P.J. (eds.) NIST Standard Reference Database Number 69. National Institute of Standards and Technology, Gaithersburg, 20899. https://doi.org/10.18434/T4D303, (retrieved March 18, 2018)

26. Dunbar, R.C., Steill, J.D., Oomens, J.: Conformations and vibrational spectroscopy of metal-ion/polyalanine complexes. Int. J. Mass Spectrom. **297**, 107–115 (2010)

27. Bongiorno, D., Ceraulo, L., Camarda, L., Ciofalo, M., Ferrugia, M., Indelicato, S., Mele, A., Liveri, V.T.: Gas-phase ion chemistry of protonated melatonin. Eur J Mass Spectrom (Chichester, Eng). **15**, 199–208 (2009)

28. Valle, J.J., Eyler, J.R., Oomens, J., Moore, D.T., van der Meer, A.F.G., von Helden, G., Meijer, G., Hendrickson, C.L., Marshall, A.G., Blakney, G.T.: Free electron laser-Fourier transform ion cyclotron resonance mass

spectrometry facility for obtaining infrared multiphoton dissociation spectra of gaseous ions. Rev. Sci. Instrum. **76**, 023103-1–023103-7 (2005)

29. Shao, Y.H., Gan, Z.T., Epifanovsky, E., Gilbert, A.T.B., Wormit, M., Kussmann, J., Lange, A.W., Behn, A., Deng, J., Feng, X.T., Ghosh, D., Goldey, M., Horn, P.R., Jacobson, L.D., Kaliman, I., Khaliullin, R.Z., Kus, T., Landau, A., Liu, J., Proynov, E.I., Rhee, Y.M., Richard, R.M., Rohrdanz, M.A., Steele, R.P., Sundstrom, E.J., Woodcock, H.L., Zimmerman, P.M., Zuev, D., Albrecht, B., Alguire, E., Austin, B., Beran, G. J.O., Bernard, Y.A., Berquist, E., Brandhorst, K., Bravaya, K.B., Brown, S.T., Casanova, D., Chang, C.M., Chen, Y.Q., Chien, S.H., Closser, K.D., Crittenden, D.L., Diedenhofen, M., DiStasio, R.A., Do, H., Dutoi, A.D., Edgar, R.G., Fatehi, S., Fusti-Molnar, L., Ghysels, A., Golubeva-Zadorozhnaya, A., Gomes, J., Hanson-Heine, M.W.D., Harbach, P.H.P., Hauser, A.W., Hohenstein, E.G., Holden, Z.C., Jagau, T.C., Ji, H.J., Kaduk, B., Khistyaev, K., Kim, J., Kim, J., King, R.A., Klunzinger, P., Kosenkov, D., Kowalczyk, T., Krauter, C.M., Lao, K.U., Laurent, A.D., Lawler, K.V., Levchenko, S.V., Lin, C.Y., Liu, F., Livshits, E., Lochan, R.C., Luenser, A., Manohar, P., Manzer, S.F., Mao, S.P., Mardirossian, N., Marenich, A.V., Maurer, S.A., Mayhall, N.J., Neuscamman, E., Oana, C.M., Olivares-Amaya, R., O'Neill, D.P., Parkhill, J.A., Perrine, T.M., Peverati, R., Prociuk, A., Rehn, D.R., Rosta, E., Russ, N.J., Sharada, S.M., Sharma, S., Small, D.W., Sodt, A., Stein, T., Stuck, D., Su, Y.C., Thom, A.J.W., Tsuchimochi, T., Vanovschi, V., Vogt, L., Vydrov, O., Wang, T., Watson, M. A., Wenzel, J., White, A., Williams, C.F., Yang, J., Yeganeh, S., Yost, S.R., You, Z.Q., Zhang, I.Y., Zhang, X., Zhao, Y., Brooks, B.R., Chan, G.K.L., Chipman, D.M., Cramer, C.J., Goddard, W.A., Gordon, M.S., Hehre, W.J., Klamt, A., Schaefer, H.F., Schmidt, M.W., Sherrill, C.D., Truhlar, D.G., Warshel, A., Xu, X., Aspuru-Guzik, A., Baer, R., Bell, A.T., Besley, N.A., Chai, J.D., Dreuw, A., Dunietz, B.D., Furlani, T.R., Gwaltney, S.R., Hsu, C.P., Jung, Y.S., Kong, J., Lambrecht, D.S., Liang, W.Z., Ochsenfeld, C., Rassolov, V.A., Slipchenko, L.V., Subotnik, J.E., Van Voorhis, T., Herbert, J.M., Krylov, A.I., Gill, P.M.W., Head-Gordon, M: Advances in molecular quantum chemistry contained in the Q-Chem 4 program package. Mol. Phys. **113**, 184–215 (2015)

30. Polfer, N.C., Oomens, J.: Vibrational spectroscopy of bare and solvated ionic complexes of biological relevance. Mass Spectrom. Rev. **28**, 468–494 (2009)

31. Mostad, A., Romming, C.: The crystal and molecular structure of N-acetyl-5-methoxy-tryptamine (melatonin). Acta Chem. Scand. B. **28**, 564–572 (1974)

32. Wakahara, A., Fujiwara, T., Tomita, K.: The crystal and molecular structure of melatonin, N-acetyl-5-methoxytryptamine. Chem. Lett. **1**, 1139–1142 (1972)

33. Mayne, L.C., Hudson, B.: Resonance Raman-spectroscopy of N-methylacetamide—overtones and combinations of the C-N stretch (amide-Ii') and effect of solvation on the C=O stretch (amide-I) intensity. J. Phys. Chem. **95**, 2962–2967 (1991)

34. Carr, J.K., Zabuga, A.V., Roy, S., Rizzo, T.R., Skinner, J.L.: Assessment of amide I spectroscopic maps for a gas-phase peptide using IR-UV double-resonance spectroscopy and density functional theory calculations. J. Chem. Phys. **140**, 224111-1–224111-9 (2014)

35. Dunbar, R.C., Steill, J.D., Polfer, N.C., Berden, G., Oomens, J.: Peptide bond tautomerization induced by divalent metal ions: characterization of the iminol configuration. Angew. Chem. **51**, 4591–4593 (2012)

36. Dunbar, R.C., Polfer, N.C., Berden, G., Oomens, J.: Metal ion binding to peptides: oxygen or nitrogen sites? Int. J. Mass Spectrom. **330**, 71–77 (2012)

37. Voronina, L., Rizzo, T.R.: Spectroscopic studies of kinetically trapped conformations in the gas phase: the case of triply protonated bradykinin. Phys. Chem. Chem. Phys. **17**, 25828–25836 (2015)

38. Bush, M.F., O'Brien, J.T., Prell, J.S., Saykally, R.J., Williams, E.R.: Infrared spectroscopy of cationized arginine in the gas phase: direct evidence for the transition from nonzwitterionic to zwitterionic structure. J. Am. Chem. Soc. **129**, 1612–1622 (2007)

39. Bush, M.F., Prell, J.S., Saykally, R.J., Williams, E.R.: One water molecule stabilizes the cationized arginine zwitterion. J. Am. Chem. Soc. **129**, 13544–13553 (2007)

40. Kamariotis, A., Boyarkin, O.V., Mercier, S.R., Beck, R.D., Bush, M.F., Williams, E.R., Rizzo, T.R.: Infrared spectroscopy of hydrated amino acids in the gas phase: protonated and lithiated valine. J. Am. Chem. Soc. **128**, 905–916 (2006)